Revista de la Sociedad Geológica de España 37 (2)

ISSN (versión impresa): 0214-2708
ISSN (Internet): 2255-1379
https://doi.org/ 10.55407/rsge.109103

NEW APPROACH TO UNDERSTANDING THE SEISMOTECTONIC REGIME OF THE BUCARAMANGA SEISMIC NEST

Nueva aproximación a la comprensión del régimen sismotectónico del nido sísmico de Bucaramanga

Pérez Jhon Leandro[1], Salcedo-Hurtado Elkin de Jesús[1], Fernández-Córdoba Jhonattan[1], Cardona-Parra César Augusto[1], García-Millán Nathalie[1]

GEORIESGO Research Group. Department of Geography, Universidad del Valle, Calle 13 # 100-00, 760042 Cali, Colombia.
leandro.perez@correounivalle.edu.co, elkin.salcedo@correounivalle.edu.co, jhonattan.fernandez@correounivalle.edu.co, cesar.augusto.cardona@correounivalle.edu.co, nathalie.garcia@correounivalle.edu.co

Abstract: *This research focuses on understanding the Bucaramanga Seismic Nest (BSN) from a physical perspective. Therefore, it does not emphasize linking its genesis with plate behavior or interaction (geodynamic perspective). It is proposed that BSN activity could be associated with the fracturing of ultramafic rocks (partially melted) whose physical mechanism of rupture is thermal shear runaway. According to the inversion of the analyzed focal mechanisms, the total stress field of BSN is compressive (R = 0.91 and R' = 2.91) and susceptible to transitioning to a transcurrent regime (permutation between σ_2 and σ_3), where medium deformation responds to a strike-slip fault with an extensional component, consistent with the estimated b value ~1.0 typical in this context. Additionally, BSN experiences high deformation rates (on the order of 10^{-5} per year), with its maximum vertical deformation rate ($z;-\dot{\varepsilon}_3 = 2.6x10^{-5}$/year) indicating a relative deformation velocity of 52 cm/year, approaching values of rising magma plumes (~200 km depth). Thus, it is suggested not to discount the possibility that seismic activity from this source could be related to some geophysical anomaly resulting from convective processes.*

Keywords: *Bucaramanga Seismic Nest, seismotectonics, focal mechanisms, stress field, thermal shear runaway.*

Resumen: *Esta investigación se enfoca en comprender el Nido Sísmico de Bucaramanga (NSB), desde una perspectiva física. Por esta razón, no enfatiza en relacionar su génesis, con la interacción de placas (perspectiva geodinámica). En este sentido, se propone que la actividad del NSB podría estar asociada con el fracturamiento de rocas ultramáficas (parcialmente fundidas) cuyo mecanismo físico de ruptura es por inestabilidad térmica. De acuerdo con la inversión de los mecanismos focales analizados, el campo de esfuerzos total del NSB es compresivo (R = 0.91 y R' = 2.91) y susceptible de cambiar a uno transcurrente (permutación entre σ_2 y σ_3), donde la deformación del medio responde a una falla de rumbo con componente extensional, consistente con el valor b estimado ~1.0 y que se relaciona con este tipo de contexto. Por otra parte, el NSB experimenta una alta deformación (del orden de 10^{-5} año^{-1}) y su máximo valor en dirección vertical ($z;\dot{\varepsilon}_3 = 2.6x10^{-5}$/*

año) tiene una velocidad relativa de deformación de 52 cm/año, aproximándose a valores de velocidad de plumas magmáticas en ascenso (~200 km de profundidad) por lo que se sugiere no descartar que la actividad sísmica de esta fuente pudiera estar relacionada con alguna anomalía geofísica que se desprenda de procesos convectivos.

Palabras clave: *Nido Sísmico de Bucaramanga, sismotectónica, mecanismos focales, campo de esfuerzos, inestabilidad térmica.*

Pérez Jhon Leandro, Salcedo-Hurtado Elkin de Jesus, Fernández-Córdoba Jhonattan; Cardona-Parra Cesar Augusto, García-Millán Nathalie, 2024. New approach to understanding the seismotectonic regime of the Bucaramanga Seismic Nest. *Revista de la Sociedad Geológica de España*, 37(2): 31-43.

Introduction

Intermediate-depth seismicity (50-300 km), unlike shallow seismicity, lacks a mainshock and does not have an aftershock pattern that follows Omori's law (exponential decay over time). Instead, it frequently occurs as clusters or "nests" (Barrett, 2015). In this context, a seismic nest is a volume where intense seismic activity is isolated from nearby activity and, unlike a "swarm" or aftershock sequence, these events persist over time (Prieto *et al.*, 2012). This seismicity occurs where temperatures and pressures exceed those expected for brittle or shear rupture mechanisms (Frohlich, 2006; Prieto *et al.*, 2012; Barrett, 2015).

The study of seismic nests can be approached from both a physical and a geodynamic perspective. In the first case, several physical rupture mechanisms have been proposed, with the most popular being dehydration embrittlement and thermal shear runaway (Frohlich, 2006; Prieto *et al.*, 2012; Barrett, 2015). In the second case, seismic nests can be generated, for example, at the edge of a plate due to contortion or tearing of the plate, or through plate overlap or collision (Nowroozi, 1971; Van der Hilst and Mann, 1994; Corredor, 2003; Cortes and Angelier, 2005; Zarifi *et al.*, 2007; Barrett, 2015). In general, scenarios involving the interaction of multiple plates are suggested to generate a seismic nest (Van der Hilst and Mann, 1994; Zarifi *et al.*, 2007; Barrett, 2015).

The Bucaramanga Seismic Nest (BSN) in Colombia, along with those of Vrancea in Romania e Hindu Kush in Afghanistan, are the most active intermediate-depth seismic sources on the planet (Zarifi and Havskov, 2003; Prieto *et al.*, 2012). From a geodynamic perspective, three broad hypotheses have been proposed regarding the genesis of the BSN beneath South America: 1) subduction of the Caribbean Plate or its tearing (Pennington, 1981; Taboada *et al.*, 2000; Corredor, 2003; Cortés and Angelier, 2005; Sánchez *et al.*, 2011; Prieto *et al.*, 2012; Vargas and Mann, 2013; Poveda *et al.*, 2015); 2) subduction of the Nazca Plate or its tearing (Van der Hilst and Mann, 1994; Chiarabba *et al.*, 2015; Wagner *et al.*, 2017); and 3) overlapping or collision of the Nazca and Caribbean plates (Zarifi *et al.*, 2007; Syracuse *et al.*, 2016; Londoño *et al.*, 2020; Cornthwaite *et al.*, 2021). From a physical perspective, some authors favor the dehydration embrittlement mechanism (Schneider *et al.*, 1987; Frohlich *et al.*, 1995; Zarifi and Havskov, 2003; Londoño *et al.*, 2020; Pérez-Forero *et al.*, 2023) while others favor the thermal shear runaway mechanism (Prieto *et al.*, 2013; Poli *et al.*, 2016).

As can be seen, various seismological studies of the BSN have primarily focused on addressing two main questions regarding the relationship of this seismic source with: 1) the interaction between plates (oceanic and continental) beneath the South American plate, and 2) the potential physical mechanisms triggering seismic activity. In this study, the seismotectonic analysis approach proposed for the BSN does not aim to relate its genesis to plate interactions; instead, it suggests a different perspective from a physical standpoint.

General seismotectonic framework

The Nazca and Caribbean oceanic plates subduct beneath the northwestern corner of South America at rates of 5.3-5.5 cm/year and 1.0-1.2 cm/year, respectively (Mora-Páez *et al.*, 2019; Mora-Páez *et al.*, 2020). This subduction generates tectonic and geological complexity within Colombian territory, manifested through the uplift of three mountain ranges, evidence of multiple fault systems, volcanism (Fig. 1), and the occurrence of earthquakes at different depth ranges (Fig. 2). The recorded seismicity in Colombia primarily ranges between 0 and 200 km in depth, concentrated along the edges of the mountain ranges where the occurrence of earthquakes is associated with crustal deformation (<50 km depth) caused by the tectonic convergence between the Nazca plate, the Northern Andean Block (NAB), the Caribbean plate, and the Panamá-Chocó Block (García-Delgado *et al.*, 2022; Martínez-Jaramillo and Prieto, 2024).

With respect to intermediate-depth seismicity, it has a latitudinal distribution pattern. In the western part of the country (~4°N), there is an occurrence of seismic events around 120 km depth (Benioff zone) that could be associated with the dehydration of the Nazca plate (Chang *et al.*, 2017; Chang *et al.*, 2019). Meanwhile, to the east (~7°N), intermediate-depth seismicity is concentrated in the central zone of the Middle Magdalena Valley (MMV), where medium-sized earthquakes (5-6M) occur at depths between

Fig. 1.- General tectonic framework of Colombia. The Nazca and Caribbean oceanic plates subduct beneath the northwestern corner of South America at rates of 5.3-5.5 cm/year and 1.0-1.2 cm/year, respectively. The Panama-Chocó Block (PCB) collides with the Northern Andes Block (NAB) at a rate of ~2.0 cm/year; the boundaries of the PCB (outlined in pink) are defined by Suter *et al.* (2008), who classify this zone as an indenter. The relative GNSS displacements are taken from Mora-Páez *et al.* (2019).

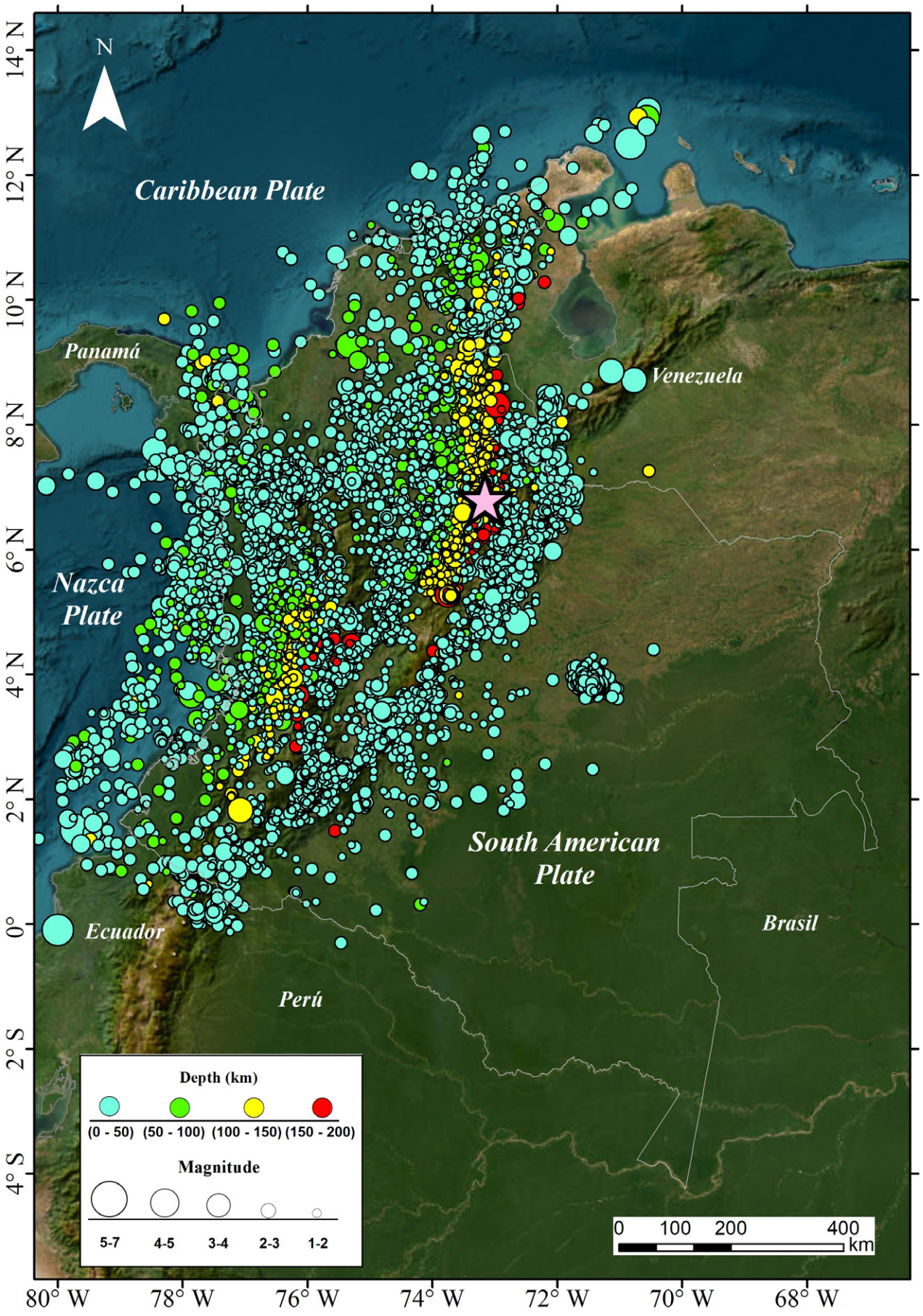

Fig. 2.- Seismicity Recorded by the Colombian Geological Service between 2013 and 2017. Seismic events with varying magnitude ranges (1–7M) and depths (0–200 km) can be observed. The magenta star represents the location of the BSN.

50 and 160 km (more than 60% of the national seismicity is recorded in this area), mainly located in the BSN (Londoño *et al.*, 2019). This seismic source, centered at 6.8°N, 73.1°W, and ~150 km depth, has the highest density of intermediate-depth seismicity in the world, expressing a high proportion of seismic events ranging from low to intermediate magnitudes, corresponding to high values of the b parameter, the occurrence of at least one ~5M earthquake per month, high stress drops, and a wide variety of focal mechanisms (Frohlich *et al.*, 1995; Zarifi and Havskov, 2003; Zarifi *et al.*, 2007; Frohlich and Nakamura 2009; Prieto *et al.*, 2012; Prieto *et al.*, 2013).

Data and methods

Data

A total of 130 seismic events with focal mechanism solutions were collected from national sources such as the Colombian Geological Service (SGC), international sources like International Seismological Centre (ISC), and previous seismological studies in the study area (Cortes and Angelier, 2005; Zarifi *et al.*, 2007; Peñaranda-Arévalo, 2023). These events occurred between January 1966 and January 2024 (58 years), with magnitudes ≥ 4.5Mw and depths ranging from 0 to 187 km (Fig. 3A).

The quadrant where the focal mechanisms are distributed includes the MMV region and the influence zone of the BSN (Fig. 3A-B). In this quadrant, 7 types of fault mechanisms are observed: pure strike-slip (SS), strike-slip with a reverse component (SS-R), reverse with a strike-slip component (R-SS), pure reverse (R), pure normal (N), normal with a strike-slip component (N-SS), and strike-slip with a normal component (SS-N). Additionally, out of the 130 focal mechanisms, 105 are in the influence zone of the BSN (81%; Fig. 4A), where there is a significant concentration of these mechanisms (71 events, corresponding to 67% of the BSN influence zone) between 140 and 160 km (Fig. 4B and Fig. 5A-B).

Methods

In this seismotectonic analysis, the kinematic and dynamic regime evaluation was considered using ternary diagrams, estimation of the b-value, calculation of the seismic strain rate, as well as determination of stress and strain fields within the observed volume of the BSN.

To delimit the area covered by the concentration (cluster) of focal mechanisms, the Kernel density estimation method was applied (Silverman, 1986). Subsequently, the general pattern of kinematic behavior in both the influence zone and clustering of the BSN was evaluated based on ter-

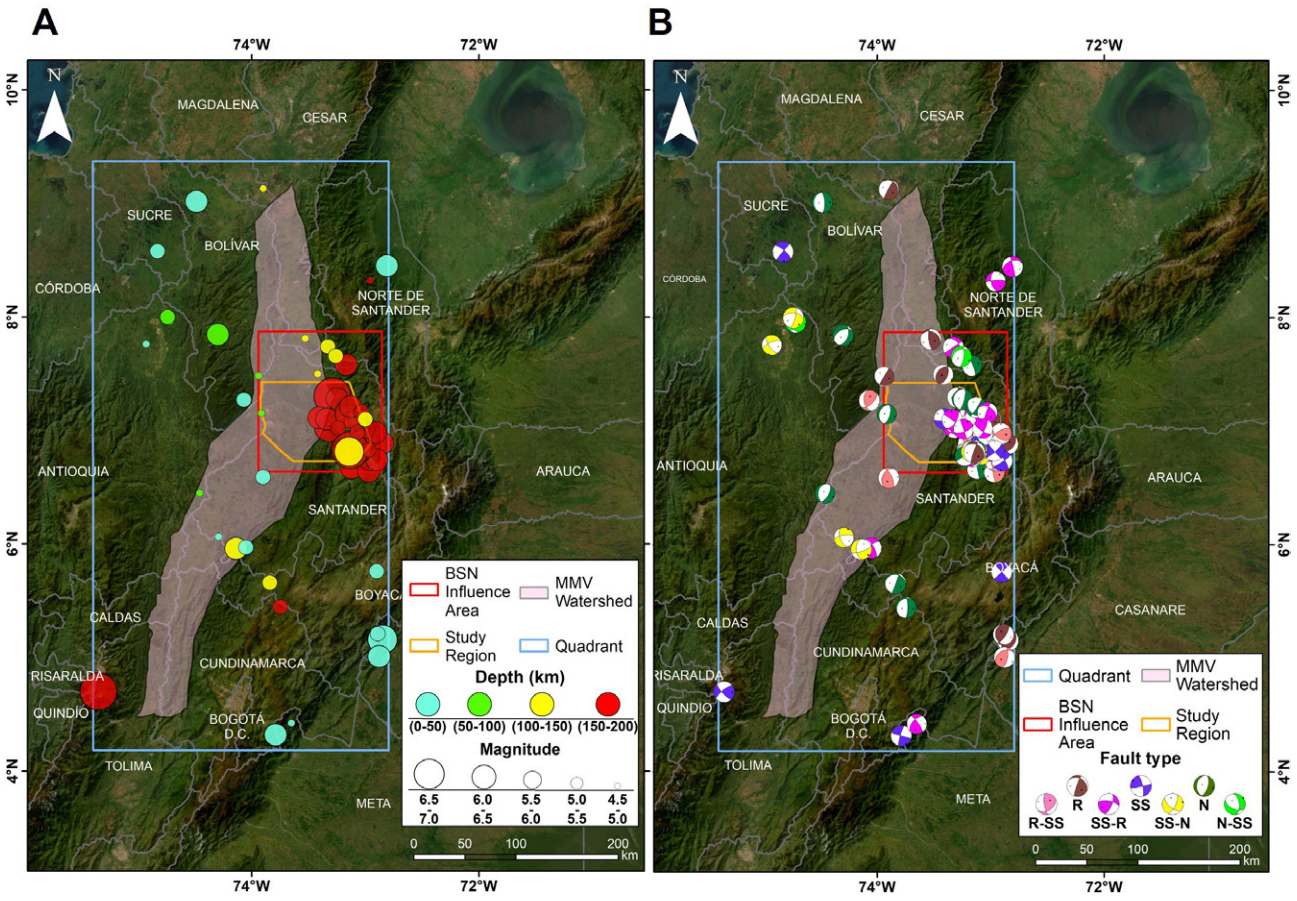

Fig. 3.- Distribution of seismicity with focal mechanism solutions in the MMV. A) Depth and magnitude of the queried seismicity. B) Focal mechanisms. The dark blue rectangle represents the general query area of the MMV, and the red square represents the influence area of the BSN, which contains the orange polygon of the study area.

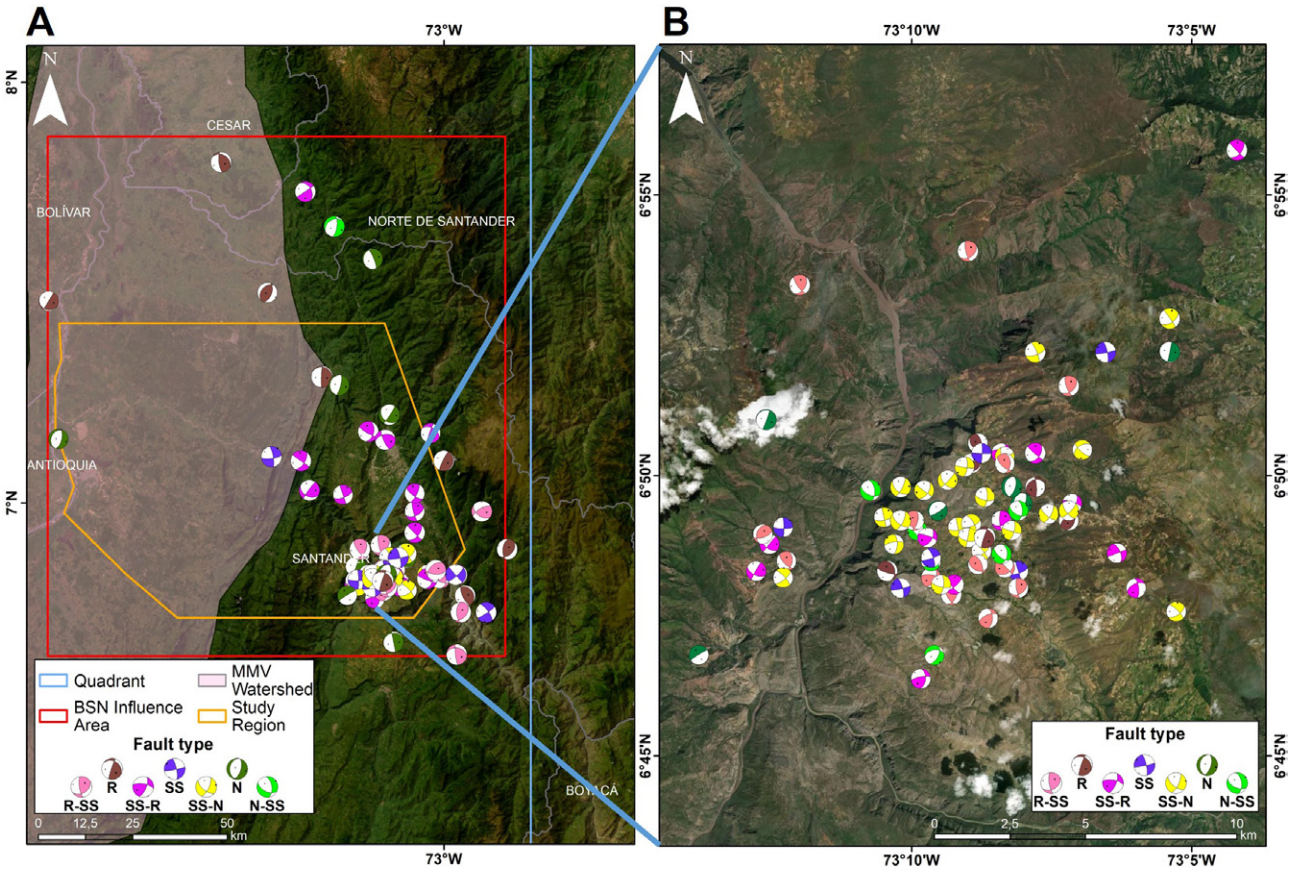

Fig. 4.- Distribution of focal mechanisms in the BSN. A) Zone of influence. B) Representation of focal mechanisms in the area where seismic events of the BSN are concentrated. A variety of mechanisms corresponding to 7 fault types are observed: pure strike-slip (SS), strike-slip with reverse component (SS-R), reverse with strike-slip component (R-SS), pure reverse (R), pure normal (N), normal with strike-slip component (N-SS), and strike-slip with normal component (SS-N). The classification of focal mechanisms follows the criteria established by Álvarez-Gómez (2014).

nary diagrams. These diagrams provide a practical way to represent the type of regime of a seismic source using fault mechanisms (Frohlich, 1992; Johnston *et al.*, 1994; Kaverina *et al.*, 1996; Kagan, 2005; Álvarez-Gómez, 2014).

The calculation of the b-value (Gutenberg and Richter, 1944; Gutenberg and Richter 1954; Aki, 1965) for the data sample was based on the method proposed by Utsu (1966). The importance of this parameter lies in its variation, which can be related to various physical processes such as high-temperature conditions, high heat flux, material heterogeneity in the observed medium, changes in rheology, variations in stress and strain states, as well as physical mechanisms of rupture (Frohlich, 2006; Prieto *et al.*, 2012; Barrett, 2015; Vargas, 2020).

The seismotectonic deformation was determined based on the concept of seismic rock flow (Riznichenko, 1965a, Riznichenko, 1965b; Kostrov, 1974). The kinematic parameters of the seismic focal mechanism are generally correlated with the direction of the deformation axes (tensor) determined within a deformed volume. The Seismotectonic Deformation Tensor (SDT) is given by the following expression:

$$\dot{\varepsilon_{ij}} = \frac{1}{2\mu VT}\sum_{n=1}^{N} M_{ij}^{n} \qquad (1)$$

Where: $\dot{\varepsilon_{ij}}$- represents the seismotectonic deformation tensor, M_{ij} denotes the components of the seismic moment tensor, V corresponds to the volume of the study area, T is the duration of seismic deformation, and μ is the rigidity modulus of the seismotectonic medium or environment.

Therefore, the SDT in a region can be calculated from the sum of the seismic moment components (M_{ij}) of a set of events within a seismically active volume (V), using a medium rigidity value ($\mu = 0.75 \times 10^{11}$ Pa; Frohlich *et al.*, 1995) over an observation period (T). In this case, the SDT of the cluster was determined, where the majority of the focal mechanisms of the NSB (67%) are concentrated over a period of T = 45 years (1979-2024), within a depth range of 140 km to 160 km (h = 20 km). The volume of the cluster is 6283 km^3 (cylinder $V = \pi r^2 h; r = 10$km).

The linear inversion method by Michael (1984), implemented in the StressInverse (Vavryčuk, 2014), was employed to calculate the stress field. By inverting the basic orientation parameters of fault planes from focal mechanism solutions (strike, dip, and rake), four parameters are obtained: the principal stress axes σ_1 (maximum compression), σ_2 (intermediate compression), σ_3 (minimum compression) and the shape factor $R = (\sigma_2 - \sigma_3) / (\sigma_1 - \sigma_3)$. This factor measures the relative magnitude of the principal stresses and indicates the type of tectonic regime that could be present (Delvaux *et al.*, 1995; Delvaux *et al.*, 1997; Ali, *et al.*, 2021).

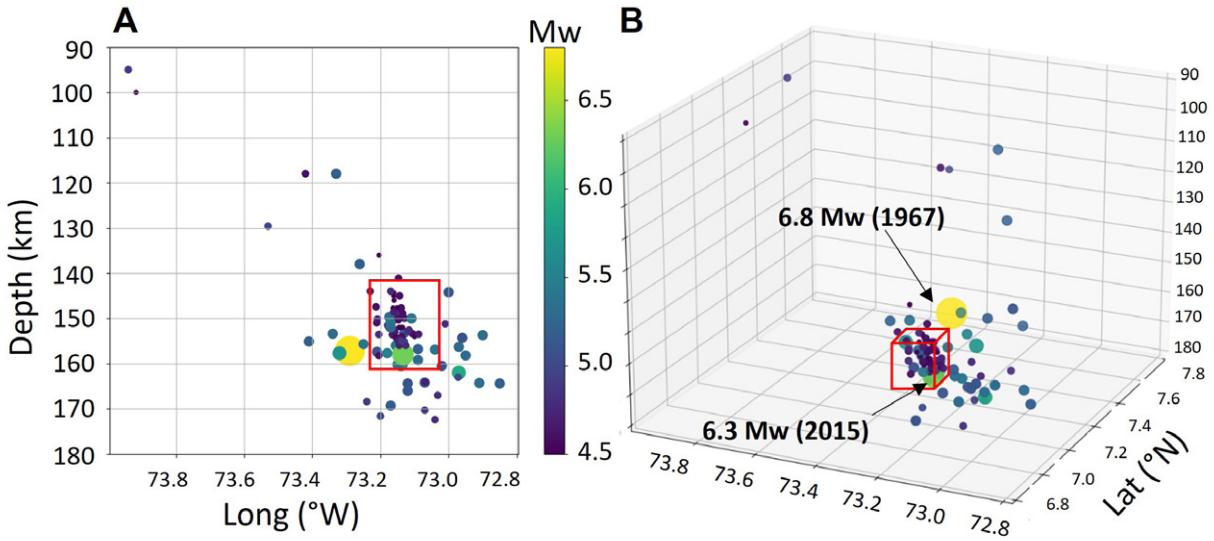

Fig. 5.- Depth distribution of seismicity in the BSN. A) 2D seismicity distribution. B) 3D seismicity distribution. Events are concentrated between 140 km and 160 km (5A). Two high-intensity earthquakes are visible (5B), with the 2015 event documented by Poli et al. (2016).

The values of R range between 0 and 1; for values around 0.5, the stress tensor is stable, whereas at the extremes, approaching 0 or 1, the tensor is unstable, and stress permutation can occur. To express the relationship and resulting stress regime more clearly, the R′ index was used (Delvaux *et al.*, 1997), which ranges from 0 to 3; R′ = R when σ_1 is vertical (extensional regime), R′ = 2 – R when σ_2 is vertical (strike-slip regime), and R′ = 2 + R when σ_3 is vertical (compressive regime). The deformation field is considered as a composite mechanism resulting from the averaging of a set of representative faults; this was estimated using the WinTensor (Delvaux and Sperner, 2003; Delvaux and Barth, 2010).

Results

Kernel density map and ternary diagrams

A kernel density map was generated to delimit the cluster of the BSN, centered at 6.8°N and -73.1°W. Within this cluster, there are 71 events within a 10 km radius (Fig. 6). The ternary diagrams display the number of mechanisms by fault type (in percentage) for both the area of influence of the BSN (Fig. 7A) and the clustering (Fig. 7B). Specifically, for this cluster, the number of mechanisms by fault type is: 6 (SS), 11 (SS-R), 13 (R-SS), 6 (R), 6 (N), 6 (N-SS) and 23 (SS-N), with the latter being the dominant fault type (see Fig. 7B and yellow beach balls in Fig. 4B).

b-Value

The b-value obtained from the data of the influence zone and clustering BSN are shown in Table 1.

BSN	b	Standard Deviation
Influence zone	1.01	0.10
Cluster	1.42	0.17

Table 1.- Estimated b value in this study for the BSN.

Seismic deformation

The seismic moment tensor is expressed as follows:

$$M_{ij} = \begin{bmatrix} -4.52 & 0.68 & 6.34 \\ 0.68 & -3.56 & -0.11 \\ 6.34 & -0.11 & 8.09 \end{bmatrix} * 10^{20} N \cdot m \quad (2)$$

From the combination of (1) and (2), it follows that TDS is:

$$\dot{\varepsilon_{ij}} = \begin{bmatrix} -1.09 & 0.16 & 1.53 \\ 0.16 & -0.86 & -0.03 \\ 1.53 & -0.03 & 1.95 \end{bmatrix} * 10^{-5} / year \quad (3)$$

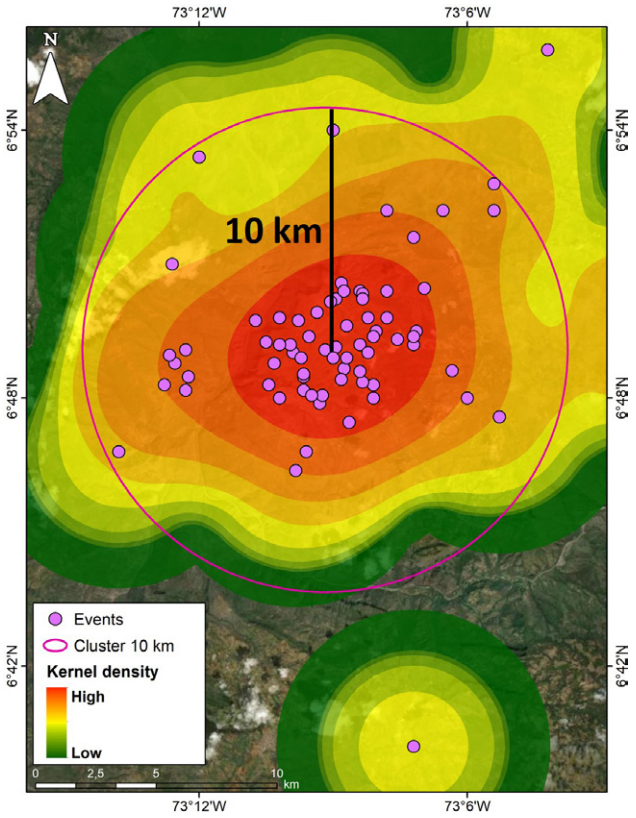

Fig. 6.- Kernel density map. The black line in the middle schematically indicates the 10 km radius length.

The eigenvalues of (3) are:

$$U = \begin{bmatrix} -1.8 \\ -0.8 \end{bmatrix} * 10^{-5} / \, year \quad (4)$$

The eigenvalues of U (in absolute magnitudes) are the principal components (x°, ε_2, ε_3) in their respective directions (x, y, z) within the analyzed volume; where (x) is in the north direction, (y) in the eastward direction, and (z) in the vertical direction toward the center of the Earth.

Thus, the maximum deformation is $2.6*10^{-5}$/year (in the vertical direction z), which results in a relative velocity of 52 cm/year ($v = h\varepsilon_3$; where h is the thickness of the volume). On the other hand, the basis for the reported deformation values in this study is close to those estimated by Frohlich *et al.* (1995) for the BSN, ranging between 10^{-6}/year and 10^{-4}/year (analysis conducted in the depth range of 140 km to 180 km with 26 focal mechanisms contrasting with values calculated by Corredor (2003) of the order of 10^{-10}/year for the Maracaibo Block, which is an area adjacent to the BSN (analysis conducted with 23 shallow crustal events at depths h ≤ 40 km).

Stress and deformation field

The Fig. 8 shows the result of the inversion of the focal mechanisms of the BSN.

σ_1 = 23/309, σ_2 = 17/211, σ_3 = 60/88
R = 0.91 y R′ = 2.91

The stress field was also discretized to observe its behavior with respect to depth (Fig. 9 and Table 2).

A complex stress regime with respect to Depth is evidenced (Fig. 9 and Table 2); from 140-145 km in the BSN, there is a compressive regime with relative stability (Fig. 9A and 9E). Between 145 and 155 km, the regime is unstable (Fig. 9B-C-F-G). Finally, at 155-160 km, there is again a compressive regime that could transition to a strike-slip regime (Fig. 9D and 9H; permutation between σ_2 and σ_3).

The composite focal mechanism calculated for the BSN represents a deformation field responding to a strike-slip fault with a normal component (SS-N; Fig. 10).

Discussion

The total stress field of the BSN is compressive (Fig. 8), and when discretized by depth range, it is observed that in the last 5 km (155-160 km), at the base of the BSN, the behavior is similar (Fig. 9D). Mohr's circles show that the compressive regime could transition to a strike-slip regime (permutation between σ_2 and σ_3, Fig. 8B and Fig. 9F-G-H). This is related to the ternary diagram of the BSN (Fig. 7), where both transtension and transpression are observed. There is a significant presence of strike-slip faults in all combinations of focal mechanisms, at least 70%.

Therefore, while the stress field affecting the BSN is compressive, the deformation primarily responds to a normal fault with a strike-slip component (Fig. 10). The calculated b-value of 1-1.4 (Table 1) specifically relates to

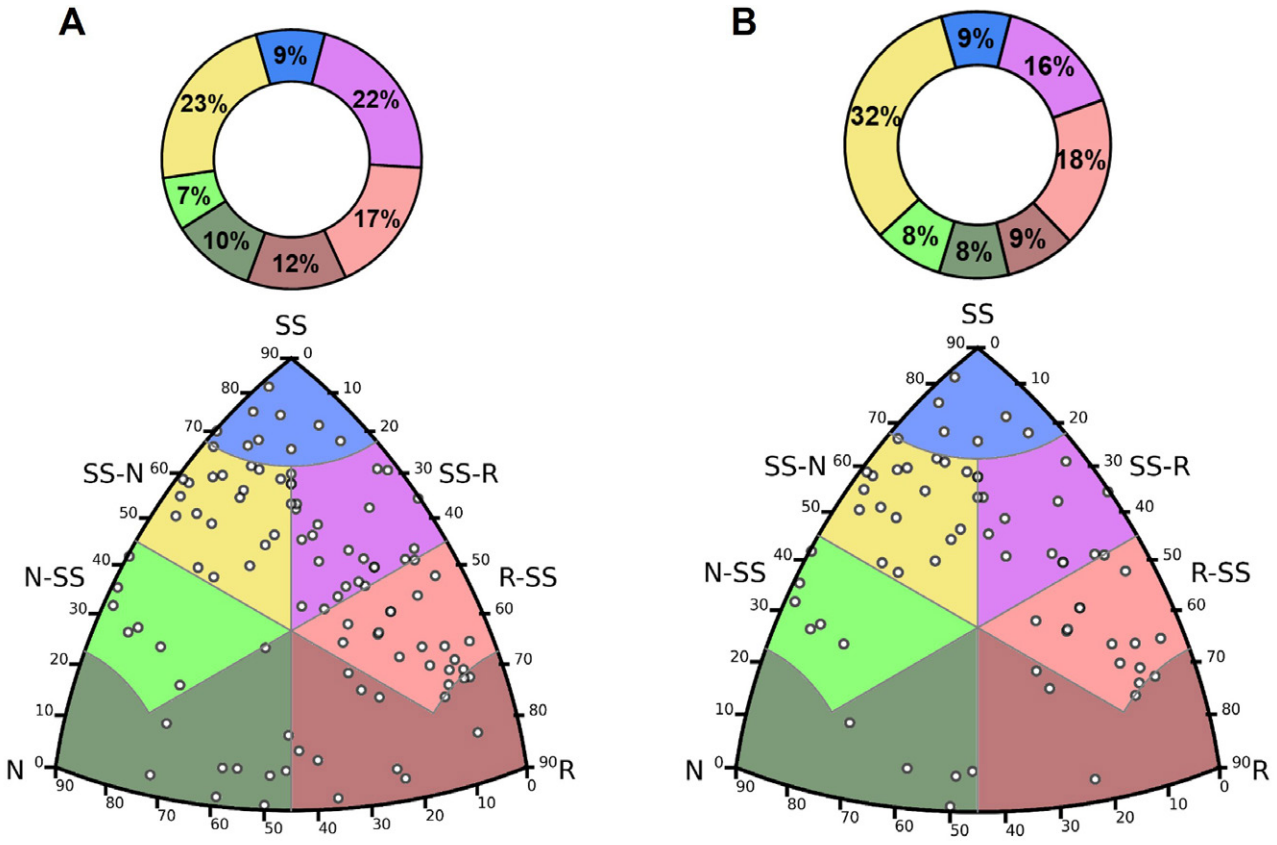

Fig. 7.- Distribution and classification of BSN event ruptures on Ternary Diagrams. A) BSN influence zone. B) BSN cluster.

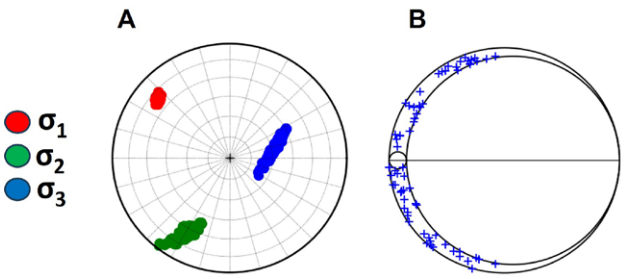

Fig. 8.- Dynamic field of the BSN. A) Total stress field of the BSN (in terms of plunge/azimuth). B) Mohr's circle.

this tectonic context (Schorlemmer *et al.*, 2005; Petruccelli *et al.*, 2019) and fits within the range (1≤b≤2) estimated by other authors for this source and its vicinity (Frohlich *et al.*, 1995; Zarifi and Havskov, 2003; Frohlich and Nakamura, 2009; Prieto *et al.*, 2012; Londoño *et al.*, 2019; Vargas, 2020). Temperature is considered a determining factor for fracturing at intermediate seismic depths; thus, the physical mechanism of thermal shear runaway is suitable to explain fault activation in the BSN, as evidenced by Prieto *et al.* (2013).

In general, the BSN experiences high deformation (on the order 10^{-5}/year), with its maximum value in the vertical component (z; $\dot{\varepsilon}_3$ = 2.6x10^{-5} per year), exhibiting a relative deformation rate of 52 cm/year within the evaluated volume. This rate is comparable to values ranging from 23 to 54 cm/year, which have been estimated for the ascent velocity of magmatic plumes at approximately 200 km depth (Turcotte and Schubert, 2014; Arnould *et al.*, 2020). Considering that the clustering of the BSN occurs between 140 and 160 km depth, it is suggested not to rule out the possibility that the seismic activity of this source could be potentially related to a geophysical anomaly resulting from convective processes.

Furthermore, given the significant occurrence of seismicity in the BSN ranging from small magnitudes (<2M and at least two earthquakes of ~4M per month) to large events (~6M), occurring between 100 and 200 km depth (Prieto *et al.*, 2012), where the medium is presumed to be viscoplastic (low-velocity zone with temperatures >1000°C; Zaccagnino and Doglioni, 2022), it leads us to consider the possibility that there may be portions or fragments of partially solidified material (interacting within the mantle), experiencing an increase in differential stresses. However, ¿what would be the origin of rocky material at these depths?

Lowrie and Fichtner (2020) propose that at depths between 100 and 200 km, there is an abundant presence of ductile silicate materials in solid state, partially or fully molten, which facilitate the movement of the rock material in the upper part of the mantle. At the same time, temperature and pressure can induce significant changes in the density and viscosity of the asthenospheric material. Despite the compositional differences between this zone and the crust, it can be considered that the composition of the materials at these depths is constant. At these conditions, due to the high temperature and relatively low pressure, large stresses are not required to achieve a certain degree non-brittle deformation. Consequently, this is a regime of plastic or viscoelastic flow, where stresses are primarily controlled by thermal activity processes.

It is possible that millions of years ago, there was a detachment of the lower part of the continental lithosphere which descended to approximately 150 km, becoming an anomalous body (high-density eclogitic drip, low poros-

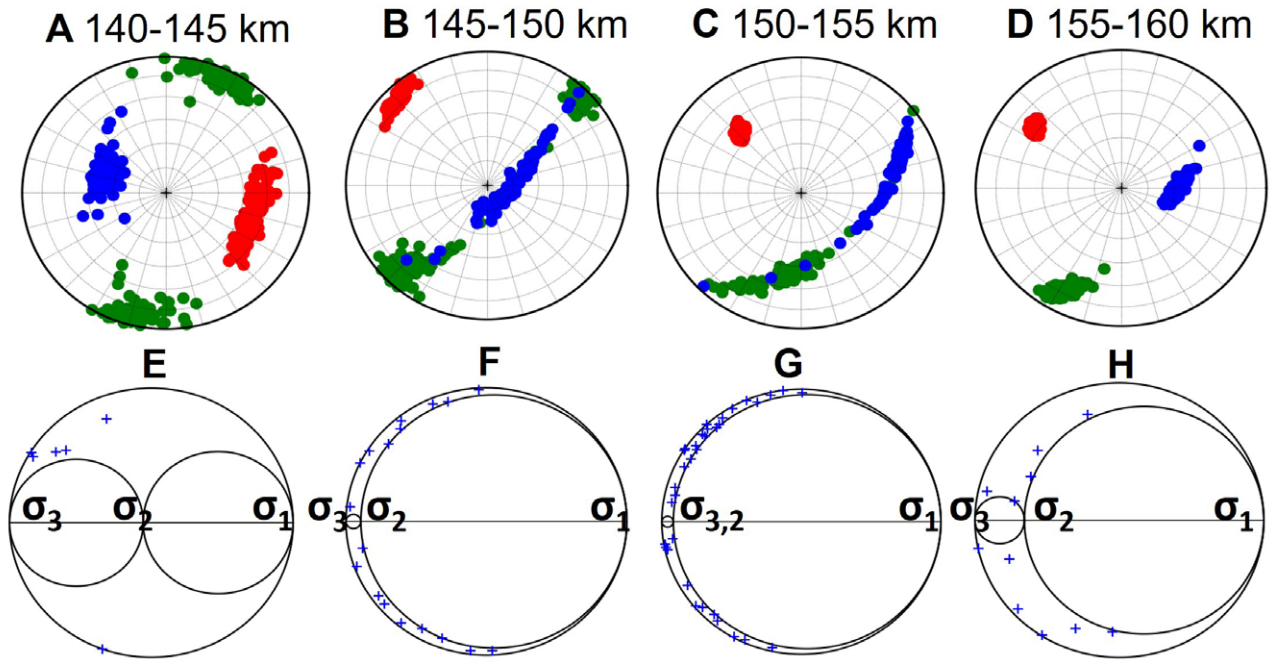

Fig. 9.- Behavior of the BSN stress field with respect to Depth (between 140 and 160 km). The upper part (first row: A, B, C, and D; σ_1 in red, σ_2 in green, and σ_3 in blue) shows the stress field by depth range (every 5 km), and the lower part (second row: E, F, G, and H) displays the corresponding Mohr's circles.

Δkm	σ_1	σ_2	σ_3	R	R′	Observation
140-145	38/109	1/199	52/290	0.5	2.50	Compressive regime relatively stable
145-150	11/312	10/220	75/88	0.9	2.9	Unstable (overlap between σ_2 and σ_3)
150-155	36/317	27/206	42/82	0.9	2.9	Unstable (overlap between σ_2 and σ_3)
155-160	26/307	18/208	57/88	0.8	2.80	Compressive regime susceptible to transitioning to strike-slip regime (permutation between σ_2 and σ_3)

Table 2.- Depth variation of principal stresses (Plunge/Azimuth) and Regime (R).

ity, and permeability) as proposed by Pérez-Forero *et al.* (2023). The presence of ultramafic rock material at these depths has been documented (Ringwood, 1991; Zaccagnino and Doglioni, 2022), consisting mainly of olivine (~51%), pyroxenes (~26% orthopyroxene and 11% clinopyroxene), and to a lesser extent, garnet (~9%). In the BSN, during the rupture process for earthquakes of 4-5Mw, there is a need for a temperature increase of 600-1000 °C (Prieto *et al.*, 2013), a range that includes, for example, the melting point of olivine and pyroxene ~1000 °C (Zaccagnino and Doglioni, 2022). This could provide further evidence supporting fracturing due to thermal shear runaway as a mechanism for intermediate-depth seismicity.

According to Wang (2016), Ben Ismaïl and Mainprice (1998), Karato *et al.* (2008), Bürgmann and Dresen (2008), the high seismicity observes in the vicinity of the BSN can be attributed to deformation mechanisms and olivine production processes that control the rheological behavior and seismic anisotropy of the upper mantle. In this context, dislocation creep and diffusion creep are the mechanisms that characterize olivine deformation (Wang *et al.*, 2018). These deformation mechanisms can operate simultaneously, but the dominant one governs the strain rate and olivine fabric.

The diffusion mechanism of olivine results from the accumulation of deformation in heated materials over extended periods. This process is governed by Fick's Law (Karato, 2008), which relates the mass flux diffused within a medium to the gradient of concentrations or pressures. As observed in the BSN, this leads to conditional deformation (Riznichenko, 1992), where stresses and strains reach their maximum values. This deformation mechanism tends to diffuse from regions of higher concentration, resembling the seismicity observed in the seismic region of the BSN. This phenomenon constitutes the seismic rock flow (Riznichenko, 1992; Kostrov, 1974; Kostrov and Das, 1988), whose maximum contribution arises from numerous small seismic events occurring in the region (Klyuchevskii and Dem'yanovich, 2015). The concept of seismic rock flow has been applied in this study to the NSB, revealing that the increase in the number of seismic events is concentrated in a small volume, where maximum stresses and absolute seismotectonic displacements occur.

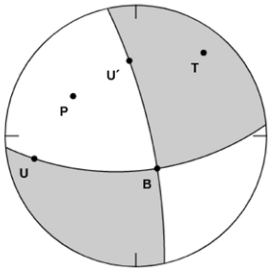

Parameters	φ	δ	λ
Plane 1	85	60	-165
Plane 2	347	77	-30
P axi	122	31	
T axi	219	11	

Fig. 10.- Deformation field of the BSN.

The complexity in understanding the seismic source of the BSN is reflected in various studies conducted to date, where there is limited correlation between results and interpretations regarding its seismotectonic analysis (Schneider *et al.*, 1987; Frohlich *et al.*, 1995; Corredor, 2003; Cortés and Angelier, 2005; Zarifi *et al.*, 2007; Londoño *et al.*, 2019; Peñaranda-Arévalo, 2023). However, the accumulated knowledge of this natural phenomenon thus far represents a valuable starting point. The BSN serves as an intriguing geophysical laboratory that should continue to be studied in the future with a multidisciplinary approach (e.g., potentially including deep magnetotelluric exploration) to enhance our understanding and contribute to the broader comprehension of Earth dynamics.

Conclusions

It is suggested that the activity of the BSN could be associated with the fracturing of ultramafic rocks (partially melted), whose rupture mechanism is due to thermal shear runaway. Additionally, it is also suggested not to discount the possibility of interaction between the BSN and anomalies resulting from convective processes (e.g., mantle plumes). On the other hand, based on the results obtained, the total stress field of the BSN is compressive and susceptible to transitioning to a transcurrent stress regime (stress permutation), where the medium deformation primarily responds to a strike-slip fault with an extensional component.

The concept of seismic rock flow, applied to the BSN region, confirms the strong concentration of small seismic events, where maximum stresses and absolute seismotectonic displacements occur. This is can also attributed to the deformation and olivine production mechanism that govern the rheological behavior and seismic anisotropy of the upper mantle. The high temperature and relatively low pressure in this zone facilitate non-brittle deformation, where stresses are generally controlled by thermal activity.

Acknowledgments and funding

We sincerely thank Dr. Stephen Johnston and the other anonymous reviewer for their constructive comments that have helped to improve the content of this paper. This Works received support from project 110287780668 titled "Seismotectonic model of the central-eastern region of the Middle Magdalena Valley as input to the knowledge of exploration and development models of hydrocarbon fields", funded through agreement 785-2019 between the National Hydrocarbons Agency, MINCIENCIAS and the Francisco José de Caldas Fund. The authors of this work thank the participating public and private entities (Industri-

al University of Santander, University of Valle, University of Pamplona, Colombian Association of Petroleum Geologists and Geophysicists, and Geofising S.A.S.), which, through contract 166 of 2021 signed with MINCIENCIAS and the partnership agreement therein, enabled the execution of this project. Additionally, we acknowledge the Vice Presidency of Research at the University of Valle, which through project CI 4425, supported the GEORIESGOS research group of the Seismological and Geophysical Observatory of Southwest Colombia (OSSO) in carrying out and completing these activities.

Author contributions

Work development, J.L.P. and E.S.; methodology, J.L.P. and E.S., data collection, J.L.P., J.F.C., C.A.C. and N.G.M.; figures, J.L.P.; research/analysis, J.L.P. and E.S.; manuscript review, J.L.P. and E.S.

References

Aki, K., 1965. Maximum likelihood estimates of b in the formula log N = a - bM and its confidence limits, Bull. Earthq. Res. Inst., 43, 237-239.

Ali, S.M., Abdelrahman, K., Al-Otaibi, N., 2021. Tectonic stress regime and stress patterns from the inversion of earthquake focal mechanisms in NW Himalaya and surrounding regions. Journal of King Saud University-Science, 33(2), 101351. https://doi.org/10.1016/j.jksus.2021.101351

Álvarez-Gómez, J.A., 2014. FMC: a one-liner Python program to manage, classify and plot focal mechanisms. Geophysical Research Abstracts, Vol. 16.

Arnould, M., Coltice, N., Flament, N., Mallard, C., 2020. Plate tectonics and mantle controls on plume dynamics. Earth and Planetary Science Letters, 547, 116439. https://doi.org/10.1016/j.epsl.2020.116439

Barrett, S.A., 2015. Seismological Constraints on the Mechanics of Intermediate-depth Earthquakes in the Bucaramanga Nest (Doctoral dissertation, Stanford University).

Ben Ismaïl, W., Mainprice, D., 1998. An olivine fabric database: An overview of upper mantle fabrics and seismic anisotropy. Tectonophysics, 296(1-2), 145-157. https://doi.org/10.1016/S0040-1951(98)00141-3

Bürgmann, R., Dresen, G., 2008. Rheology of the lower crust and upper mantle: Evidence from rock mechanics, geodesy, and field observations. Annu. Rev. Earth Planet. Sci., 36(1), 531-567. https://doi.org/10.1146/annurev.earth.36.031207.124326

Chang, Y., Warren, L.M., Prieto, G.A., 2017. Precise locations for intermediate-depth earthquakes in the Cauca cluster, Colombia. Bulletin of the Seismological Society of America, 107(6):2649–2663. https://doi.org/10.1785/0120170127

Chang, Y., Warren, L., Zhu, L., Prieto, G.A., 2019. Earthquake focal mechanisms and stress field for the intermediate-depth Cauca cluster, Colombia. Journal of Geophysical Research: Solid Earth, 124(1):822-836. https://doi.org/10.1029/2018JB016804

Chiarabba, C., De Gori, P., Faccenna, C., Speranza, F., Seccia, D., Dionicio, V., Prieto, G.A., 2015. Subduction system and flat slab beneath the Eastern Cordillera of Colombia. Geochemistry, Geophysics, Geosystems, 17(1), 16-27. https://doi.org/10.1002/2015GC006048

Cornthwaite, J., Bezada, M.J., Miao, W., Schmitz, M., Prieto, G.A., Dionicio, V., Levander, A., 2021. Caribbean slab segmentation beneath northwest South America revealed by 3-D finite frequency teleseismic P-wave tomography. Geochemistry, Geophysics, Geosystems, 22(4). https://doi.org/10.1029/2020GC009431

Corredor, F., 2003. Seismic strain rates and distributed continental deformation in the northern Andes and three-dimensional seismotectonics of northwestern South America. Tectonophysics, 372(3-4), 147-166. https://doi.org/10.1016/S0040-1951(03)00276-2

Cortés, M., Angelier, J., 2005. Current states of stress in the northern Andes as indicated by focal mechanisms of earthquakes. Tectonophysics, 403(1-4), 29-58. https://doi.org/10.1016/j.tecto.2005.03.020

Delvaux, D., Moeys, R., Stapel, G., Melnikov, A., Ermikov, V., 1995. Palaeostress reconstructions and geodynamics of the Baikal region, Central Asia, Part I. Palaeozoic and Mesozoic pre-rift evolution. Tectonophysics, 252(1-4), 61-101.

Delvaux, D., Moeys, R., Stapel, G., Petit, C., Levi, K., Miroshnichenko, A., San'kov, V., 1997. Paleostress reconstructions and geodynamics of the Baikal region, central Asia, Part 2. Cenozoic rifting. Tectonophysics, 282(1-4), 1-38. https://doi.org/10.1016/S0040-1951(97)00210-2

Delvaux, D., Sperner, B., 2003. New aspects of tectonic stress inversion with reference to the Tensor program. Geol Soc London Spec Publ, 212:75–100. https://doi.org/10.1144/GSL.SP.2003.212.01.06

Delvaux, D., Barth, A., 2010. African stress pattern from formal inversion of focal mechanism data. Tectonophysics 482:105-128. https://doi.org/10.1016/j.tecto.2009.05.009

Frohlich, C., 1992. Triangle diagrams: ternary graphs to display similarity and diversity of earthquake focal mechanisms. Physics of the Earth and Planetary interiors, 75(1-3), 193-198. https://doi.org/10.1016/0031-9201(92)90130-N

Frohlich, C., 2006. Deep earthquakes. Institute for Geophysics, Jackson School of Geosciences University of Texas at Austin. 592p. https://doi.org/10.1017/CBO9781107297562

Frohlich, C., Kadinsky-Cade, K., Davis, S.D., 1995. A reexamination of the Bucaramanga, Colombia, earthquake nest. Bulletin of the Seismological Society of America, 85(6), 1622-1634.

Frohlich, C., Nakamura, Y., 2009. The physical mechanisms of deep moonquakes and intermediate-depth earthquakes: How similar and how different? Physics of the Earth and Planetary Interiors, 173(3-4), 365-374. https://doi.org/10.1016/j.pepi.2009.02.004

Garcia-Delgado, H., Velandia, F., Bermúdez, M.A., Audemard, F., 2022. The present-day tectonic regimes of the Colombian Andes and the role of slab geometry in intraplate seismicity. International Journal of Earth Sciences, 111(7), 2081-2099. https://10.1007/s00531-022-02227-9

Gutenberg, B., Richter, C.F., 1944. Frequency of earthquakes in California. Bulletin of the Seismological Society of America, 34 (4): 185-188. https://doi.org/10.1785/BSSA0340040185

Gutenberg, B., Richter, C.F., 1954. Magnitude and energy of earthquakes, Ann. Geofis., 9, 1-15. https://doi.org/10.4401/ag-5590

Johnston, A.C., Kanter, L.R., Coppersmith, K.J., Cornell, C.A., 1994. The earthquakes of stable continental regions. Volume 1, Assessment of large earthquake potential, Final report No. EPRI-TR-102261-V1. United States: N. Web. https://www.epri.com/research/products/TR-102261-V1

Kagan, Y.Y., 2005. Double-couple earthquake focal mechanism: random rotation and display. Geophysical Journal International 163, 1065-1072. https://doi.org/10.1111/j.1365-246X.2005.02781.x

Karato, S.I., 2008. Deformation of Earth Materials. An Introduction to the Rheology of Solid Earth. 463 p. https://doi.org/10.1017/S0016756809006323

Karato, S.I., Jung, H., Katayama, I., Skemer, P., 2008. Geodynamic significance of seismic anisotropy of the upper mantle: New insights from laboratory studies. Annu. Rev. Earth Planet. Sci., 36(1), 59-95. https://doi.org/10.1146/annurev.earth.36.031207.124120

Kaverina, A.N., Lander, A.V., Prozorov, A.G., 1996. Global creepex distribution and its relation to earthquake-source geometry and tectonic origin. Geophysical Journal International 125 (1), 249-265. https://doi.org/10.1111/j.1365-246X.1996.tb06549.x

Klyuchevskii, A.V., Dem'yanovich, V.M., 2015. The 3D seismotectonic flow of geological masses in the lithosphere of the Baikal Rift Zone. Journal of Volcanology and Seismology. 9, 48-64. https://doi.org/10.1134/S0742046315010042

Kostrov, B.V., 1974. Seismic moment and energy of earthquakes and seismic flow of rock. Izv. Acad. Sci. USSR Earth Phys. 1, 23-44.

Kostrov, B.V., Das, S., 1988. Principles of earthquake source mechanics. Cambridge University Press. 286 p.

Londoño, J.M, Quintero, S., Vallejo, K., Muñoz, F., Romero, J., 2019. Seismicity of Valle Medio del Magdalena basin, Colombia. Journal of South American Earth Sciences, 92, 565-585. https://doi.org/10.1016/j.jsames.2019.04.003

Londoño, J.M, Vallejo, K., Quintero, S., 2020. Detailed seismic velocity structure of the Caribbean and Nazca Plates beneath Valle Medio del Magdalena region of NE Colombia. Journal of South American Earth Sciences, 103, 102762. https://doi.org/10.1016/j.jsames.2020.102762

Lowrie, W., Fichtner, A., 2020. Fundamentals of geophysics. Cambridge University Press. 419 p. https://doi.org/10.1017/9781108685917

Martínez-Jaramillo, D., Prieto, G.A., 2024. Tectonic setting of the northwestern andes Constrained by a high-resolution earthquake catalog: Block Kinematics. Journal of South American Earth Sciences, 134, 104761. https://doi.org/10.1016/j.jsames.2023.104761

Michael, A.J., 1984. Determination of stress from slip data: faults and folds. Journal of Geophysical Research: Solid Earth, 89 (B13):11517-11526. https://doi.org/10.1029/JB089iB13p11517

Mora-Páez, H., Kellogg, J.N., Freymueller, J.T., Mencin, D., Fernandes, R.M., Diederix, H., Corchuelo-Cuervo, Y., 2019. Crustal deformation in the northern Andes–A new GPS velocity field. Journal of South American Earth Sciences, 89, 76-91. https://doi.org/10.1016/j.jsames.2018.11.002

Mora-Páez, H., Kellogg, J.N., Freymueller, J.T., Gómez, J., Pinilla-Pachon, A.O., 2020. Contributions of space geodesy for geodynamic studies in Colombia: 1988 to 2017.The Geology of Colombia, 4, 479-498. https://doi.org/10.32685/pub.esp.38.2019.14

Nowroozi, A.A., 1971. Seismotectonics of the Persian plateau, eastern Turkey, Caucasus, and Hindu-Kush regions, Bullet. Seism. Soc. Am., 61, (2), 317-341.

Peñaranda, A.W.E., 2023. Inversión del tensor de momentos de eventos pertenecientes al nido sísmico de Bucaramanga utilizando datos regionales. (Tesis de Maestría). Universidad Industrial de Santander. Colombia. https://noesis.uis.edu.co/handle/20.500.14071/14409

Pennington, W.D., 1981. Subduction of the eastern Panama Basin and seismotectonics of northwestern South America. Journal of Geophysical Research: Solid Earth, 86(B11), 10753-10770. https://doi.org/10.1029/JB086iB11p10753

Pérez-Forero, D., Koulakov, I., Vargas, C.A., Gerya, T., Al Arifi, N., 2023. Lithospheric delamination as the driving mechanism of intermediate-depth seismicity in the Bucaramanga Nest, Colombia. Scientific Reports, 13(1), 23084. https://doi.org/10.1038/s41598-023-50159-4

Petruccelli, A., Schorlemmer, D., Tormann, T., Rinaldi, A.P., Wiemer, S., Gasperini, P., Vannucci, G., 2019. The influence of faulting style on the size-distribution of global earthquakes. Earth and Planetary Science Letters, 527, 115791. https://doi.org/10.1016/j.epsl.2019.115791

Poli, P., Prieto, G.A., Yu, C.Q., Florez, M., Agurto-Detzel, H., Mikesell, T.D., Pedraza, P., 2016. Complex rupture of the M 6.3 2015 March 10 Bucaramanga earthquake: Evidence of strong weakening process. Geophysical Journal International, 205(2), 988-994. https://doi.org/10.1093/gji/ggw065

Poveda, E., Monsalve, G., Vargas, C.A., 2015. Receiver functions and crustal structure of the northwestern Andean region, Colombia. Journal of Geophysical Research: Solid Earth, 120(4), 2408-2425. https://doi.org/10.1002/2014JB011304

Prieto, G.A., Beroza, G.C., Barrett, S.A., López, G.A., Florez, M., 2012. Earthquake nests as natural laboratories for the study of intermediate-depth earthquake mechanics. Tectonophysics, 570, 42-56. https://doi.org/10.1016/j.tecto.2012.07.019

Prieto, G.A., Florez, M., Barrett, S.A., Beroza, G.C., Pedraza, P., Blanco, J.F., Poveda, E., 2013. Seismic evidence for thermal runaway during intermediate-depth earthquake rupture. Geophysical Research Letters, 40(23), 6064-6068. https://doi.org/10.1002/2013GL058109

Ringwood, A.E., 1991. Phase transformations and their bearing on the constitution and dynamics of the mantle. Geochimica et Cosmochimica Acta, 55(8), 2083-2110. https://doi.org/10.1016/0016-7037(91)90090-R

Riznichenko, Yu.V., 1965a. Seismic rock flow, in: Dinamika zemnoi kory (Dynamics of the Earth's Crust). Nauka, Moscow, 56–63 (in Russian).

Riznichenko, Yu.V., 1965b. Relationship between the seismic flow of the rock mass and seismicity. Report of the Academy of Sciences of the USSR, 161(1), 97-99 (in Russian).

Riznichenko, Yu.V., 1992. Problems of seismology: selected papers. Mir Publishers. 462 p. https://doi.org/10.1007/978-3-662-09446-4

Sánchez, J., Götze, H.J., Schmitz, M., 2011. A 3-D lithospheric model of the Caribbean-South American plate boundary. International Journal of Earth Sciences, 100, 1697-1712. https://doi.org/10.1007/s00531-010-0600-8

Schneider, J.F., Pennington, W.D., Meyer, R.P., 1987. Microseismicity and focal mechanisms of the intermediate-depth Bucaramanga Nest, Colombia. Journal of Geophysical Research 92, 13913-13926. https://doi.org/10.1029/JB092iB13p13913

Schorlemmer, D., Wiemer, S., Wyss, M., 2005. Variations in earthquake-size distribution across different stress regimes. Nature 437, 539-542. https://doi.org/10.1038/nature04094

Silverman, B.W. 1986. Density estimation for statistics and data analysis. In: Monographs on Statistics and Applied Probability 26. Chapman and Hall, London. 177 p.

Suter, F., Sartori, M., Neuwerth, R., Gorin, G., 2008. Structural imprints at the front of the Chocó-Panamá indenter: Field data from the North Cauca Valley Basin, Central Colombia. Tectonophysics, 460(1-4), 134-157. https://doi.org/10.1016/j.tecto.2008.07.015

Syracuse, E.M., Maceira, M., Prieto, G.A., Zhang, H., Ammon, C.J., 2016. Multiple plates subducting beneath Colombia, as illuminated by seismicity and velocity from the joint inversion of seismic and gravity data. Earth and Planetary Science Letters, 444, 139-149.

https://doi.org/10.1016/j.epsl.2016.03.050

Taboada, A., Rivera, L.A., Fuenzalida, A., Cisternas, A., Philip, H., Bijwaard, H., Rivera, C., 2000. Geodynamics of the northern Andes: Subductions and intracontinental deformation (Colombia). Tectonics, 19(5), 787-813. https://doi.org/10.1029/2000TC900004

Turcotte, D., Schubert, G., 2014. Geodynamics. Cambridge University Press. https://doi.org/10.1017/CBO9780511843877

Utsu, T., 1966. A statistical significance test of the difference in b-value between two earthquake groups. Journal of Physics of the Earth, 14(2), 37-40. https://doi.org/10.4294/jpe1952.14.37

Van der Hilst, R., Mann, P., 1994. Tectonic implications of tomographic images of subducted lithosphere beneath northwestern South America, Geology, 22, 451-454. https://doi.org/10.1130/0091-7613(1994)022%3C0451:TIOTIO%3E2.3.CO;2

Vargas, C.A., 2020. Subduction geometries in northwestern South America. In: Gómez, J. and Pinilla-Pachon, A.O. (editors), The Geology of Colombia, Volume 4 Quaternary. Servicio Geológico Colombiano, Publicaciones Geológicas Especiales. 397-422. Bogotá. https://doi.org/10.32685/pub.esp.38.2019.11

Vargas, C.A., Mann, P., 2013. Tearing and breaking off of subducted slabs as the result of collision of the Panama Arc-Indenter with northwestern South America. Bulletin of the Seismological Society of America, 103(3), 2025-2046. https://doi.org/10.1785/0120120328

Vavryčuk, V., 2014. Iterative joint inversion for stress and fault orientations from focal mechanisms. Geophysical Journal International, 199(1), 69-77. https://doi.org/10.1093/gji/ggu224

Wagner, L.S., Jaramillo, J. S., Ramírez-Hoyos, L.F., Monsalve, G., Cardona, A., Becker, T.W., 2017. Transient slab flattening beneath Colombia. Geophysical Research Letters, 44(13), 6616-6623. https://doi.org/10.1002/2017GL073981

Wang, Q., 2016. Homologous temperature of olivine: Implications for creep of the upper mantle and fabric transitions in olivine. Science China Earth Sciences, 59, 1138-1156. https://doi.org/10.1007/s11430-016-5310-z

Wang, S., Yu, H., Zhang, Q., Zhao, Y., 2018. Absolute plate motions relative to deep mantle plumes. Earth Planet. Sci. Lett.490, 88-99. https://doi.org/10.1016/j.epsl.2018.03.021

Zaccagnino, D., Doglioni, C., 2022. Earth's gradients as the engine of plate tectonics and earthquakes. La Rivista del Nuovo Cimento, 45(12), 801-881. https://doi.org/10.1007/s40766-022-00038-x

Zarifi, Z., Havskov, J., 2003. Characteristics of dense nests of deep and intermediate-depth seismicity. Advances in geophysics, 46, 238-278. https://doi.org/10.1016/s0065-2687(03)46004-4

Zarifi, Z., Havskov, J., Hanyga, A., 2007. An insight into the Bucaramanga nest. Tectonophysics, 443(1-2), 93-105. https://doi.org/10.1016/j.tecto.2007.06.004

MANUSCRITO RECIBIDO: 30-07-2024
REVISIÓN RECIBIDA: 24-10-2024
ACEPTACIÓN DEL MANUSCRITO REVISADO: 11-12-2024